DESIGN AND TESTING OF A RIG TO INVESTIGATE BUOYANCY-INDUCED HEAT TRANSFER IN AERO-ENGINE COMPRESSOR ROTORS

Dario Luberti **Marios Patinios** **Richard W. Jackson** **Hui Tang**

Oliver J. Pountney **James A. Scobie** **Carl M. Sangan** **J. Michael Owen**

Gary D. Lock

Department of Mechanical Engineering, University of Bath
Bath, BA2 7AY, United Kingdom

ABSTRACT

The change in compressor blade-tip clearance across the flight cycle depends on the expansion of the rotor, which in turn depends on the temperature and stress in the discs. The radial distribution of temperature is directly coupled to the buoyancy-driven flow and heat transfer in the rotating disc cavities. This paper describes a new test rig specifically designed to investigate this conjugate phenomenon. The rig test section includes four rotating discs enclosing three cavities. Two discs in the *central* cavity are instrumented with thermocouples to provide the radial distribution of temperature; the two *outer* cavities are thermally insulated to create appropriate boundary conditions for the heat transfer analysis. An axial throughflow of air is supplied between a stationary shaft and the bore of the discs. The temperature of the throughflow air is measured by thermocouples in rakes upstream and downstream of the central cavity. For a cold throughflow, the outer shroud of the central cavity is heated. Two independently-controlled radiant heaters allow differential shroud temperatures for the upstream and downstream discs, as found in aero-engine compressors. Alternatively, the throughflow can be heated above the shroud temperature to simulate the transient conditions during engine operation where stratified flow can occur inside the cavity. The rig is designed to operate in conditions where both convective and radiative heat transfer dominate; all internal surfaces of the cavity are painted matt black to allow the accurate calculation of the radiant heat transfer. Separate attachments can be fitted to the cobs of both central discs; the attachments reduce the axial gap between the cobs – reducing the gap to zero creates a closed cavity, which can occur in some compressor designs. Other instrumentation includes heat-flux gauges on the shroud and high-frequency pressure transducers embedded into the disc diaphragm to capture unsteady flow structures. Attention has been given to experimental uncertainty, including the computation of the thermal-disturbance errors, caused by thermocouples embedded in the rotating discs; a Bayesian statistical model is used to reduce the effect of uncertainties in temperature measurements on the calculation of the Nusselt number. The effect of relevant non-dimensional parameters on the radial distribution of the disc and throughflow temperatures has been shown for some typical cases.

NOMENCLATURE

a	inner radius of disc [m]
b	outer radius of disc [m]
b'	outer radius of diaphragm [m]
d_h	hydraulic diameter (= $2(a - r_s)$) [m]
$\dot{m}$	mass flow rate [kg/s]
r	radius [m]
r_s	radius of shaft [m]
$r\vartheta$	circumferential position [mm]
s	axial gap at the cavity inlet [m]
T	temperature [K]
W	axial throughflow velocity [m/s]
β	volume expansion coefficient [K^{-1}]
μ	dynamic viscosity [m^2/s]
ρ	density [kg/m^3]
Ω	angular velocity [rpm]

Dimensionless parameters

Bo	buoyancy number (=$Re_\phi^2 \beta\Delta T/ Re_z^2$)
G	gap ratio (= s/b)
Gr	Grashof number (= $Re_\phi^2 \beta\Delta T$)
Re_z	axial Reynolds number (= $\rho_f W d_h/\mu_f$)
Re_ϕ	rotational Reynolds number (= $\rho_f \Omega b^2/\mu_f$)
Ro	Rossby number (= $W/\Omega a$)
$\beta\Delta T$	buoyancy parameter (= $(T_{o,b} - T_f)/T_f$)
Θ	non-dimensional temperature (= $(T_o - T_f)/(T_{o,b'} - T_f)$)

Subscripts

$b;\ b'$	value at $r = b;$ value at $r = b'$
f	value in axial throughflow
o	value on disc surface
z	axial direction
ϕ	circumferential direction

1. INTRODUCTION

Future generations of aero-engines are targeting ever greater overall pressure ratios (OPR) to improve efficiency and meet

environmental legislation. The OPR of compressors have increased from 30:1 in the 1970s to 60:1 in current engine designs, with plans to increase to 70:1 to meet Advisory Council for Aeronautics Research and Innovation in Europe (ACARE) targets by 2025. This creates a challenge to the designer: higher OPR require smaller compressor blades in the last stages of the high-pressure compressor (HPC); this increases the sensitivity of the compressor efficiency and stability margin to the blade tip clearance across the flight cycle (idle, take-off, climb, cruise, descent and approach).

Figure 1 is a conceptual illustration of an HPC featuring a stack of co-rotating discs and cavities. The primary flow of air through the outer annulus is compressed through blades and vanes and heat is transferred to the shrouds of the cavities. Secondary air extracted from upstream stages creates (in the steady-state) a relatively cool axial throughflow in the annular gap between the disc cobs and the shaft. Buoyancy-induced flow occurs inside the open rotating cavities formed by the co-rotating discs and shroud, with an exchange of enthalpy and momentum between the throughflow and the air inside the cavity. The blade-tip clearance across the flight cycle is governed by the expansion of the compressor rotor, which in turn depends on the radial distribution of temperature and stress in the discs. This is a conjugate problem in which the radial distribution of temperature is directly coupled to the buoyancy-driven flow and heat transfer in the rotating disc cavities.

As illustrated in Figure 1, the flow can be broadly divided into two convection regions. The axial throughflow has a strong influence in the region near the cobs, and the size of this region is governed by the Rossby Number (Ro), defined as the ratio of the mean axial throughflow velocity to the rotational speed of the discs:

$$\mathrm{Ro}=\frac{W}{\Omega a}\propto\frac{\mathrm{Re}_z}{\mathrm{Re}_\phi} \tag{1}$$

All symbols are defined in the nomenclature. Typically, Ro < 1 under engine conditions. The outer convection region is governed by buoyancy. The buoyant effect can be quantified in non-dimensional terms by the Grashof number (Gr), which combines the contribution of rotation (substituting gravity with the centripetal acceleration) and temperature difference:

$$\mathrm{Gr}=\mathrm{Re}_\phi^2\beta\Delta T \tag{2}$$

where Re_ϕ is the rotational Reynolds number and $\beta\Delta T$ the buoyancy parameter:

$$\mathrm{Re}_\phi=\frac{\rho\Omega b^2}{\mu_f} \tag{3}$$

$$\beta\Delta T=\frac{T_{o,b}-T_f}{T_f} \tag{4}$$

At engine conditions, Gr ~ 10^{13}. The buoyancy number (Bo) is the ratio of buoyancy to Coriolis forces and useful in determining the relative dominance of forced to free convection in the cavity:

$$\mathrm{Bo}=\frac{\mathrm{Re}_\phi^2\beta\Delta T}{\mathrm{Re}_z^2} \tag{5}$$

Buoyancy-induced flow, which is intrinsically three - dimensional and unstable, presents a challenge for computational fluid dynamics, and CFD cannot achieve accurate results at the high Gr found in modern compressors. Many engine designers are therefore forced to rely on empirical equations and physically-based theoretical models.

This paper describes the design and commissioning of a new compressor-cavity rig built to explore and investigate the buoyancy-induced flow and heat transfer phenomena associated with aero-engines. Section 2 provides a review of the literature relevant to compressor cavity rigs. Sections 3 and 4 describe the design features and instrumentation of the new rig at the University of Bath. A thermal and stress analysis is presented in Section 5. Radial distributions of disc temperature over a range of Ro, Re_ϕ and Gr are shown in Section 6 as part of the commissioning tests for the rig. The data demonstrates the starting point for a full systematic investigation of the flow and heat transfer inside compressor cavities at both steady-state and transient conditions. The conclusions are discussed in Section 7.

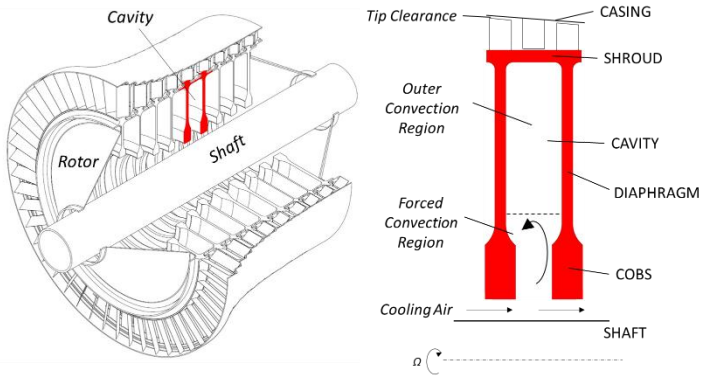

FIGURE 1. Typical aero-engine HPC (left) with a 2D sketch of the rotating cavity (right) illustrating two convection regions.

2. LITERATURE REVIEW

A review of buoyancy-induced flow in rotating cavities, including details of several experimental rigs, is given by Owen and Long [1]. They concluded that, for a given geometry, Gr, Re_ϕ, Ro, and $\beta\Delta T$ are the most important non-dimensional parameters. Bo, the buoyancy number, is a parameter useful in determining the transition from forced to free convection in the cavity. For large values of Ro, the axial throughflow, which generates a toroidal vortex in the cavity, can significantly affect the flow and heat transfer; vortex breakdown could also occur. For small values of Ro and large values of Gr (which usually occur at steady-state conditions in aero-engines), buoyancy-induced flow dominates; this tends to create large-scale unsteady vortex structures in the cavities. For negative values of Gr, which can occur during engine accelerations and decelerations when the throughflow is hotter than the shroud, the flow can become

thermally stratified; under these conditions, there would be a rapid reduction in heat transfer from the shroud and discs. The descriptions below relate to papers not discussed in that review [1] or to those that are of direct relevance to the present study.

Günther *et al.* [2-3] also found evidence for the presence of two convection regions (see Figure 1), one influenced by buoyancy, the other by the axial throughflow featuring a toroidal vortex. Experiments were conducted in a two-cavity rig with a uniformly heated external shroud operating over the range $Re_\phi < 9.3\times10^6$, $Re_z < 1.2\times10^5$, and $Gr < 2.3\times10^{13}$. Both cavities were instrumented, with thermocouples distributed across the rotating surface of one disc. The heat flux was determined from the axial-temperature gradient across the disc. In both cavities there was a radius where the heat flux approached zero; this was at higher a radius in the first cavity where impingement of the throughflow was stronger. This was identified as the point where the heat flux cancelled at the boundary between the two convection regions.

Quan *et al.* [4] also used a two-cavity rig to characterize the heat transfer in the following ranges: $0.2 < Ro < 1.6$, $0.16 < \beta\Delta T < 0.3$, $4.7\times10^{10} < Gr < 9.8\times10^{11}$. The distributions of heat transfer coefficient were obtained through specific sensors developed in-house. The measurements indicated the presence of a region affected by forced convection and a region dominated by buoyancy. Once again, the axial throughflow affects mainly the cob region, especially the downstream disc.

A recent single cavity rig described by Diemel *et al.* [5] aims to measure the cavity surface temperature, surface pressure, core temperature and inlet swirl angle over a range of non-dimensional parameters. The rig features high rotational speed with $Re_\phi \sim 1.4\times10^7$ and $Gr < 10^{14}$. Both discs are instrumented with thermocouples located on two surfaces and the authors plan to perform finite element analysis using interpolated temperatures to extract the heat fluxes and therefore the heat transfer coefficients. (As far as the authors are aware, no results have yet been published.)

The multi-cavity rig at the University of Sussex is a 70% model of a high-pressure aero-engine compressor. Various builds of the facility have been used to make the most important contributions to understanding the flow and heat transfer in compressor rotors. The first build of the rig is described by Alexiou [6]; the rig features two cavities and a cone, instrumented with thermocouples embedded in the metal surfaces and a rotating shaft. Impinging hot air was used to heat the shroud and the cooling air could be pressurized to increase the rig performance in terms or Re_z, Re_ϕ and Gr. Long and others [7-10] reported extensive experiments on velocity measurements (using laser-Doppler-velocimetry) in the fluid core and heat transfer to the discs and shroud on later builds of the rig (with up to five cavities).

Atkins and Kanjirakkad [11] used the Sussex rig to investigate the effects of the relevant nondimensional parameters on the disc temperature distribution ($0.3 < Ro < 4.7$, $0.06 < \beta\Delta T < 0.32$, $5.4\times10^8 < Gr < 2.9\times10^{12}$). Both sides of a single disc were instrumented with thermocouples, and most of the tests showed that the axial-variation of temperature was within the uncertainty limits of the measured values.

Tang *et al.* [12] used the application of Bayesian statistics to the inverse solutions of the circular fin equation, to determine Nusselt numbers for rotating discs. The method was successfully applied to determine the Nusselt numbers (and their confidence intervals) from the experimental disc-temperature measurements of Atkins and Kanjirakkad [11]. As there was little axial variation of the temperatures, they used the average value, which assumed that the Nusselt numbers were the same on either surface of the disc. In practice, this is unlikely to be correct, and the authors suggested that future experiments should be conducted with discs where one surface is thermally insulated. They also showed that calculating Nusselt numbers from finite-difference solutions of Laplace's equation (which many experimenters have done and continue to do) is an error-prone method resulting in nonphysical oscillations in the calculated values. The Bayesian model and insulated discs are used in the experiments conducted in the new compressor-cavity rig described below.

A summary of the maximum Grashof number (Gr) and buoyancy parameter ($\beta\Delta T$) for the most recent and relevant compressor-cavity rigs is shown in Figure 2.

3. DESIGN OF THE RIG

The Bath compressor-cavity rig includes many of the features found in the Sussex rig described in Section 2. However,

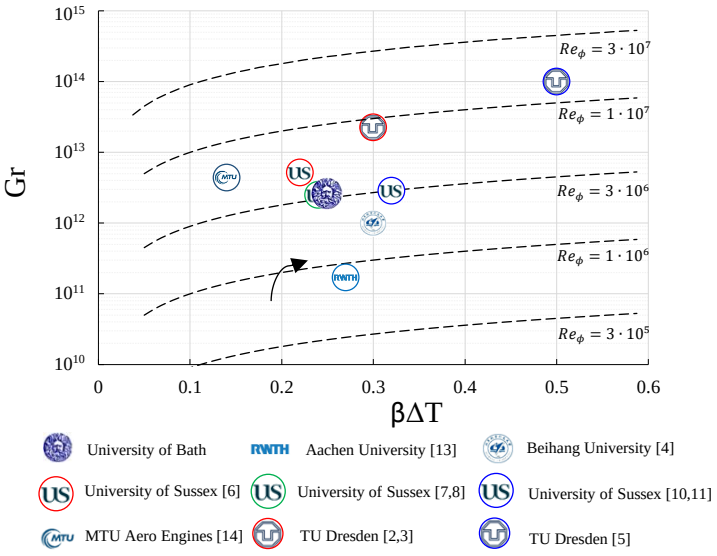

FIGURE 2. Grashof number and buoyancy parameter capabilities for recent rigs in literature; iso-Re_ϕ lines are shown.

although it is a three-cavity rig, disc and shroud temperatures are measured only in the central cavity; the surfaces of the outer cavities are thermally insulated to avoid the ambiguity (noted above) in the calculation of the disc Nusselt numbers associated with uninsulated discs. This is an important design feature directly supporting the use of the fin model [12], which implicitly assumes there are no axial temperature differences within the disc; the zero axial temperature gradient is equivalent

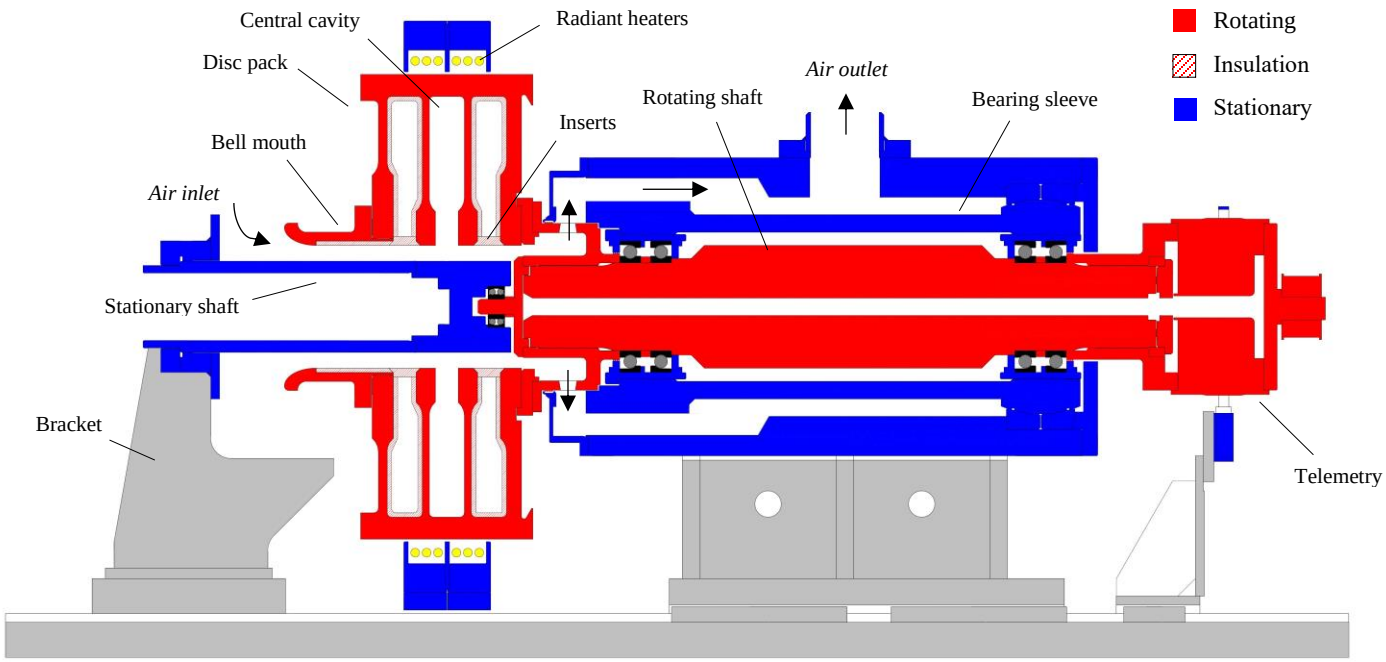

FIGURE 3. Compressor-Cavity Rig at the University of Bath.

to a symmetry axis on the insulated surface. The rig includes other features not found in (or not reported for) the rigs described in Section 2. The shroud can be differentially heated to produce temperature differences between the upstream and downstream discs, as found in operating compressors. Also, measurements of temperature can be obtained on both upstream and downstream discs simultaneously.

The cob geometry can be readily changed, and the axial throughflow can be heated to produce negative values of $\beta\Delta T$, which could be used to determine when stratified flow occurs inside the cavity. In these cases, or when buoyancy effects are weak, radiation between the internal surfaces of the cavity can be significant. So that any radiant heat transfer can be accurately calculated, these surfaces are painted with matt black paint.

Careful consideration was also given to the analysis of the data and to the estimation of the uncertainties in the calculated Nusselt numbers. As this is an inverse problem, in which small uncertainties in the temperature measurement lead to very large uncertainties in the calculated heat fluxes, a Bayesian statistical model was used to calculate the fluxes; details of this are given in the paper by Jackson *et al.* [15]. As buoyancy -induced flow is a conjugate problem, in which the conduction in the discs is coupled to convection in the air inside the cavity, the Bayesian model was used in conjunction with a one-dimensional circular fin equation for the conduction solution. This model not only provides an estimate of the radial distribution of the Nusselt numbers, it also provides the 95% confidence interval for these estimates and the associated standard deviation for the radial distribution of the temperature measurements themselves. These uncertainties are dependent on the number of thermocouples used to measure the radial distribution of disc temperature – 28 were used on each disc in the rig - and the Bayesian estimates of the uncertainties in the temperature distribution is more meaningful than the estimated uncertainty of an individual thermocouple. That is, knowing or believing that a single temperature can be calculated with an uncertainty of, say, 0.5° C is meaningless within the context of calculating the Nusselt numbers. (Many experimenters believe that the oscillations in their computed Nusselt numbers have a physical significance whereas in all probability the oscillations were caused by the method of analysis used for this inverse problem.)

Figure 3 is a cross-sectional view of the Bath Compressor-Cavity Rig, which was designed and constructed in partnership with Torquemeters Ltd. The rotating and stationary components are marked red and blue respectively. The drive unit features a super-critical design, where the rotating shaft spins the disc pack through a spline. The shaft is supported by two bearings contained within a sleeve, itself located within an external casing and frame. The radial movement of the shaft is dampened by four springs at the disc end. The downstream end (right-hand side) of the shaft is equipped with a telemetry unit supplied by Datatel. At the left-hand side, a stationary shaft is located within a bracket, while the rotating shaft is supported by a small bearing.

Tang *et al.* [16] noted that the rotational speed of the central shaft appeared to have no significant effect on the heat transfer from the discs in the Sussex multi-cavity rig. This observation is consistent with the paper of Long and Childs [8] who saw no significant effect of the shaft rotation on the heat transfer from the shroud in their experiments. For this reason, a stationary shaft was used in the Bath compressor-cavity rig.

The air flow is left to right, entering the rig through an aluminum bell-mouth inlet and creating an axial throughflow in

the annular gap between the disc cobs and the stationary central shaft. By means of an extraction unit, the air passes through the drive-shaft assembly via radial holes; a labyrinth seal reduces leakage/ingress to < 1% of the throughflow rate.

An isometric view of the rig is shown in Figure 4 with the air inlet, disc pack, drive-shaft assembly and air outlet to the extractor shown. The throughflow is set by a variable speed Becker (SV300/1, 7.5 kW) extraction unit for mass flow rates up to 0.15 kg/s, measured by a Bronkhorst thermal meter to within +/- 0.0005 kg/s. The throughflow can be heated to investigate cases with negative values of Gr, which can occur during engine accelerations and decelerations when this throughflow is hotter than the shroud.

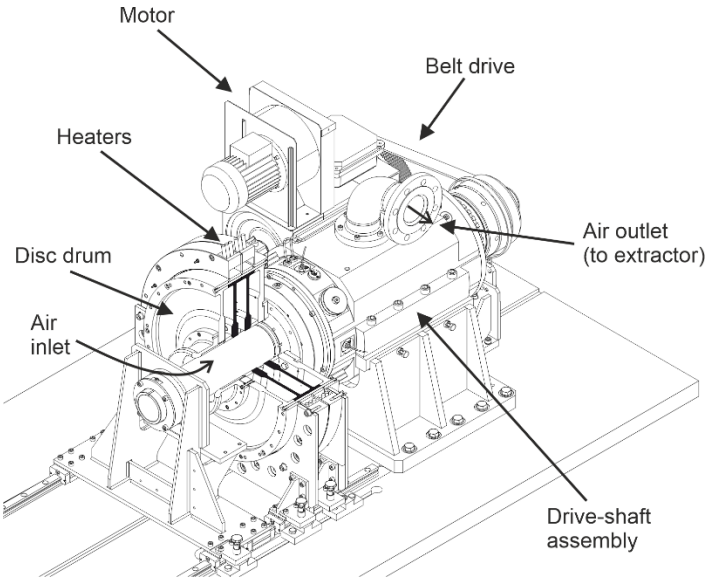

FIGURE 4. Overview of Compressor-Cavity Rig.

In the test section of the rig, four bolted titanium (Ti-6Al-4V) discs enclose three cavities: upstream, central and downstream. The two central discs are instrumented with thermocouples and heat flux-gauges for measurements in the central cavity. The back surfaces of these discs, in the upstream and downstream cavities, were insulated with Rohacell, a low-conductivity machinable foam (thermal conductivity 0.03 W/mK); the insulation was bonded to the titanium surfaces using Loctite EA9794. For the tests reported here, enthalpy and momentum exchange to the upstream and downstream cavities is prevented by modular, Rohacell inserts; these were held in place and located by a spigot. The shroud is heated by two sets of circumferential radiant heaters (2 kW each); these can be independently controlled and allow differential shroud temperatures for the central discs. Typical under-shroud temperatures are 100 °C; this temperature is limited by the thermal properties of the thermal insulation and, as discussed in Section 5, the allowable stress in the rotating discs.

Figure 5 shows the current operating limits of the Bath compressor-cavity rig in terms of Gr, $\beta\Delta T$, Ro and Re_z. The boundaries are determined by the maximum rotational speed (fundamentally limited to stresses in the discs), the maximum operating temperature of the insulating materials, and the limitation on the throughflow rate. The rig is designed to capture engine-representative data between Gr ~ 10^{12} and Gr ~ 10^{10}. The lower value (which corresponds to the lowest feasible rotational speed of 800 rpm) is useful for CFD computations when LES (Large Eddy Simulation) is used.

Modularity and flexibility have been addressed by the design of the rig. A rail system allows movement of the disc pack relative to the drive unit and access to the test section. Separate aluminium attachments can be fitted to the cobs of both central discs; the attachments reduce the axial gap between the cobs - reducing the gap to zero creates a closed cavity, which exists in some compressor designs. Figure 6 illustrates the three cob

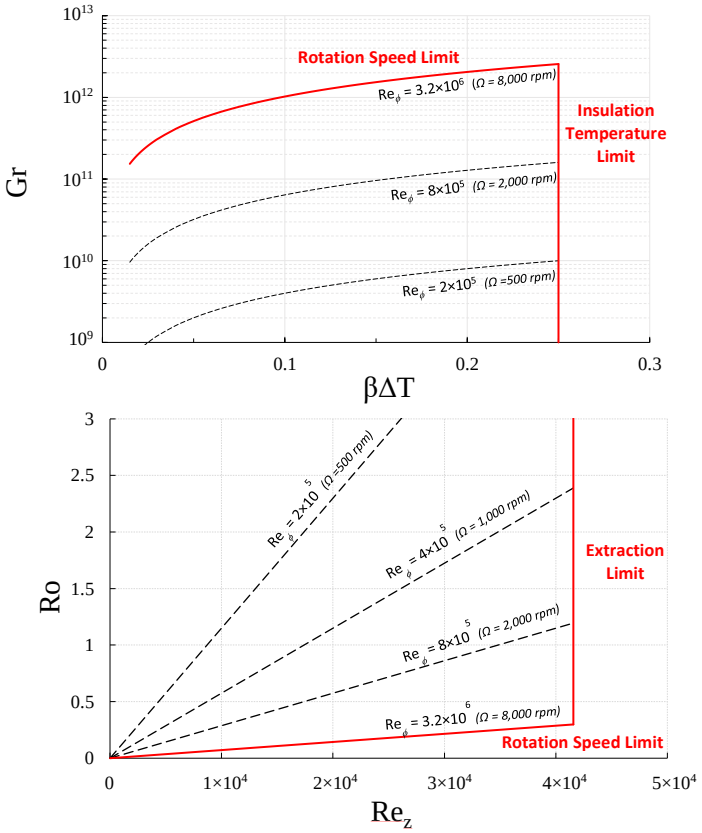

FIGURE 5. Buoyancy-Induced Flow rig operating limits: Grashof number and buoyancy parameter (top); Rossby number and axial throughflow Reynolds number (bottom).

geometries that can be tested and defines the principal dimensions of the test section. Symbols are further defined in the

nomenclature. Rig geometric details and operating parameters are summarized in Table 1.

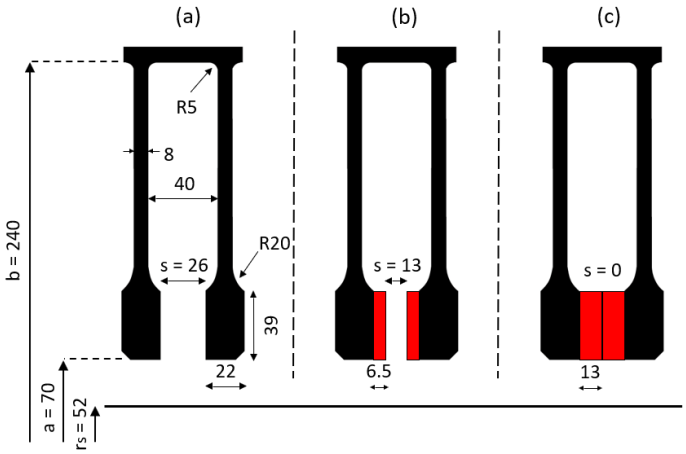

FIGURE 6. Geometrical dimensions of the cavity and possible cob configurations. Dimensions in mm.

Shroud radius	b [mm]	240
Cavity ratio	a/b	0.29
Shaft radius ratio	r_s/a	0.74
Gap ratio	s/b	0 – 0.11
Rotational speed	Ω [rpm]	800 – 8000
Mass flow rate	$\dot{m}$ [kg/s]	0 – 0.15
Shroud temperature (max)	$T_{b,max}$ [°C]	100
Rotational Reynolds number (max)	$Re_{\phi,max}$	3.2×10^6
Axial Reynolds number (max)	$Re_{z,max}$	4×10^4
Rossby number	Ro	0.1 – 3
Buoyancy parameter (max)	$\beta\Delta T_{max}$	0.25
Grashof number (max)	Gr_{max}	2×10^{12}

TABLE 1. Rig geometrical and operating parameters.

4. INSTRUMENTATION

This section first describes the use of thermocouples on the rotating discs, including methods to minimise thermal disturbance. The routing of the instrumentation to the telemetry unit is also discussed. In the stationary frame of reference, the temperature of the throughflow air is measured using thermocouples in rakes upstream and downstream of the central cavity.

4.1 Rotating instrumentation

A cross-section of the test section (for no cob attachments) and the instrumentation on the discs is shown in Figure 7. Note that the four discs in the co-rotating stack are listed Disc 1 to 4 in the downstream direction, with Discs 2 and 3 forming the central cavity. Both discs feature a radial distribution of 28 thermocouples across the cob and diaphragm regions. The radii and relative circumferential locations of the measurements are further illustrated in Figure 8. The thermocouples were made in-house from a single AWG36 (0.13 mm diameter) batch of K-type thermocouple wire pairs (Omega GG-KI-36-SLE). The ends of the wires were welded using a SR80 universal welder to form a bead with a diameter < 0.4 mm.

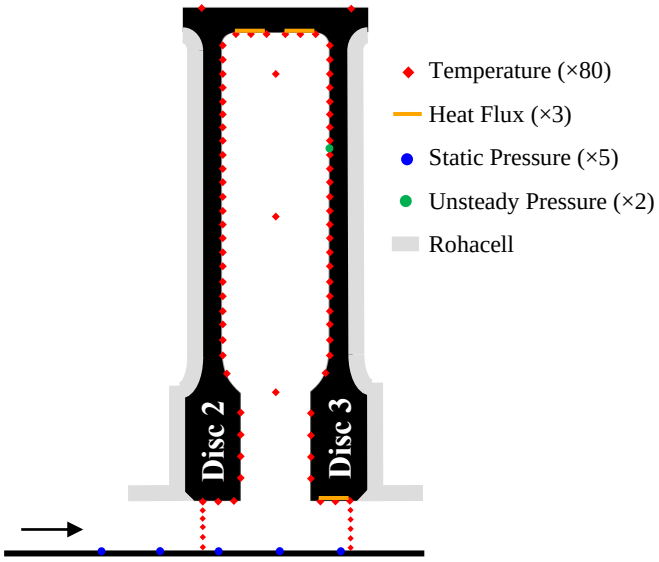

FIGURE 7. Overview of cavity instrumentation.

Figure 9 illustrates the circumferential grooves (slots) machined into the titanium discs for the thermocouples and how the wires were passed through the disc to the back surface, from where they are routed radially outward and eventually to the telemetry system. The thermocouples were arranged in bundles and passed freely through axial holes in the shroud to the back face of Disc 4. Slack in the cables was secured under a "lip" machined on the shroud of Disc 4; this slack ensured that the discs could be separated when adding or removing the cob attachments. The thermocouple wires were potted directly in the narrow portion of the slot, singly insulated in the wider portion, and double insulated in the through-hole and beyond. The shape of the slots on the disc surface was designed to reduce local stress concentrations as discussed in Section 5.

The slot grooves were designed to span an isotherm at constant radius as the temperature distribution on the disc surfaces were assumed axisymmetric. The thermocouple junctions were placed at the end of the slot, flush with the surface, and the slot was then filled with epoxy resin. The thermal-disturbance error was minimised in two ways. Firstly, the amount of resin in the vicinity of the junction was reduced by sizing the slot to be as small as possible; the end of the slot is rounded with a radius of 0.5 mm. Secondly, the epoxy resin was specifically selected to satisfy both adhesive criteria (sheer and peel strength) and thermal conductivity; the latter should ideally

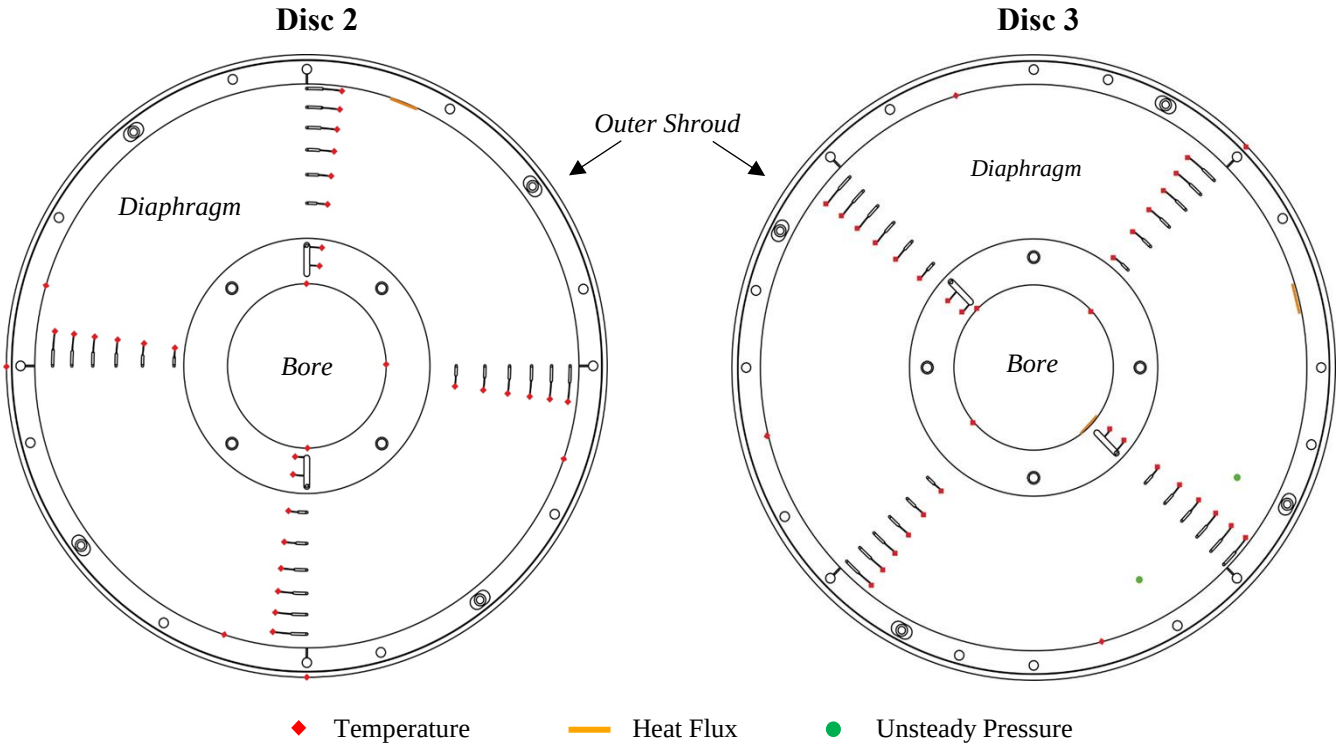

FIGURE 8. Instrumentation locations on the discs

match the titanium (see Table 2). Appendix 1 describes the finite-element analysis that was used to estimate the magnitude of the thermal-disturbance error. The maximum error was found to be < 0.25 °C, which is less than the uncertainty of the temperature measurement.

In addition to the thermocouples on the disc surfaces, three thin-foil thermocouples were secured to the underside of the cobs at the bore and to the inner surface of the shrouds. Also at the bore and shroud were three RdF 27160-C-L-A01 thermopile heat flux gauges, each individually calibrated for steady-state measurements between 0.5 – 8 kW/m^2 and gauge temperatures up to 110 °C. These gauges each had 54 thermopile junctions made from copper-constantan pairs; the thickness and thermal conductivity of the polyimide film used to separate the junctions were unknown and their values were determined by a maximum likelihood estimate based on the experimental calibration.

Two fast-response (100 kHz) unsteady pressure sensors (Kulite XCQ-080, range 1.5 bara) were installed into the surface of Disc 3 in order to determine the unsteady cyclonic/anti-cyclonic structures in the cavity.

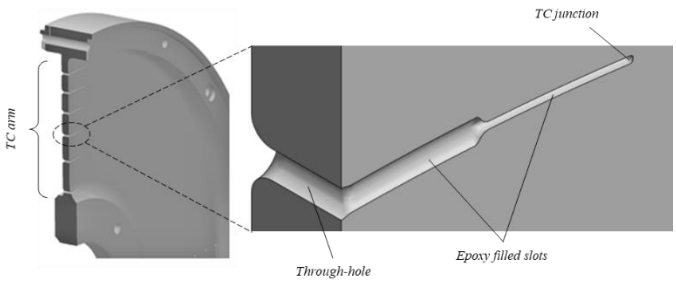

FIGURE 9. Thermocouple slot details.

Titanium (Ti-6Al-4V)	
Density [kg/m^3]	4620
Young's modulus [GPa]	96
Poisson's ratio	0.36
Yield strength [MPa]	889
Thermal expansion coefficient [°C^{-1}]	9.4×10^{-6}
Thermal conductivity [Wm^{-1}K^{-1}]	7
Epoxy resin (cured)	
Density (settled) [kg/m]	~2000
Young's modulus [GPa]	2.4
Thermal expansion coefficient [°C^{-1}]	50×10^{-6}
Thermal conductivity [Wm^{-1}K^{-1}]	1.4
Shear strength on steel	9 N/mm^2

TABLE 2. Relevant mechanical and thermal properties of titanium and epoxy resin.

4.2 Stationary instrumentation

Figure 7 shows that the air temperature of the throughflow at the inlet and outlet of the central cavity were measured by means of rakes, each with five thermocouples evenly spaced in

the annulus between the stationary shaft and the disc bore. The pressure drop for the throughflow was recorded through five static pressure sensors (ESI Technology Ltd. PR3204) in the stationary shaft.

In future tests, the temperature and the pressure in the cavity core will be measured at various radial locations by one of two stationary instrumented probes, attached to the central shaft; one probe contains K-type thermocouples and the other unsteady pressure sensors (Kulite XCQ-080, range 1.5 bara). To reduce the drag on the probes and the disturbance of the rotating core, each probe has a symmetrical aerofoil section. Future experiments will also involve modifications to incorporate a radial inflow bleed to the instrumented cavity.

A Table showing the distribution of the instrumentation is shown in Appendix 2.

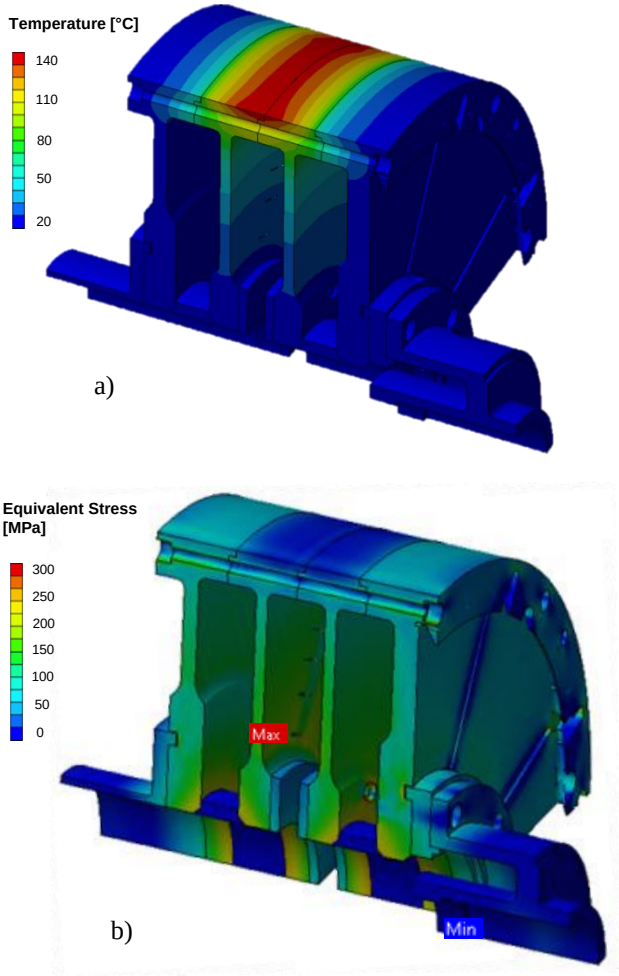

FIGURE 10. Finite element analysis results; a) temperature field, b) equivalent stress.

4.3 Data acquisition system

The wires for the rotating instrumentation were routed to a telemetry unit at the drive-end of the shaft. Six separate modules within the Datatel telemetry unit were able to handle 71 thermocouple and heat flux gauge signals (at 10 Hz), plus two 10 kHz signals (for the fast-response pressure transducers). All the thermocouple signals were cold-junction compensated through a locally-installed Pt100 Resistance Temperature Detector (RTD). The uncertainty in the temperature of the cold junction is estimated to be ± 0.2 °C. All thermocouples were made from the same batches of chromel and alumel wires; a sample was calibrated in a water bath up to 100ºC, and the standard deviation from the NIST standard was 0.1ºC. The data was transmitted to a receiver using an antenna; the overall uncertainty of the temperature acquired from the rotating thermocouples following compensation was estimated to be ± 0.5 °C, at a 1σ confidence level.

5. THERMAL AND STRESS ANALYSIS

The rig has been designed for the following conditions: rotational speeds up to 8000 rpm; a maximum temperature of 100 °C for the inner surface of the shroud; and an operating life of at least 10^4 cycles. Prior to experimental tests, a finite element three-dimensional thermo-mechanical analysis was performed using Ansys v18 to validate the design against these requirements. Due to symmetry, only a quarter sector of the disc pack was modeled. Each rotating disc was subjected to individual centrifugal and thermal stresses. When assembled as a disc pack, the presence of multiple constraints altered the stress and deformation modes.

5.1 Thermal Analysis

Thermal finite element analysis was conducted using a mesh with 1.6 million elements for the case of cob attachments (Figure 6b) under the following boundary conditions: maximum temperature difference between the inner shroud (100 °C) and the bore (20 °C) and with all insulated surfaces considered adiabatic; cylinder convection correlations were used for the external shrouds of Disc 1 and Disc 4 [17]; a free-disc convection correlation was used for the outer surfaces of the disc pack; and heat transfer coefficients on the inner shroud and on the cavity surfaces were determined using the Owen-Tang buoyancy model [18].

The computed temperature field is shown in Figure 10a. The radial gradient of temperature was strongest near the shroud. There was also a substantial axial decay of temperature on the shroud. These two effects combined to constrain the expansion of Discs 2 and 3, and influenced the deformation and stress discussed below.

5.2 Stress Analysis

A stress analysis, using a symmetrically-heated shroud, was conducted under two loads: the mechanical model at a rotational speed of 8000 rpm and the thermal load from the thermal solution. The deformation from the analysis is illustrated in Figure 10b, with smoothed contours of equivalent (von Mises) stress. The maximum value of stress was found on the disc diaphragm (owing to the bending mode) where the machined slots, which allow flush-mounted thermocouple junctions and through-holes, act as local stress raisers. Mesh refinements were concentrated in the areas of maximum stress. Principal

material/mechanical data for titanium Ti-6Al-4V is shown in Table 2.

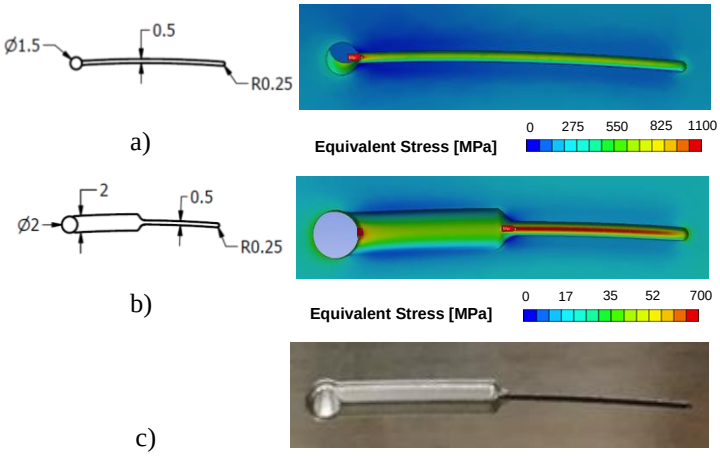

FIGURE 11. Thermocouple slot geometry design and stress: (a) original, (b) final, (c) photograph after manufacturing. The depth is constant and 0.5 mm for both grooves.

The slot geometry shown in Figure 9 evolved from a simpler design with a machined slot of uniform width. The computed stress for the original and final design is shown in Figure 11a and b respectively. Figure 11c is a photograph of the machined slot in the titanium disc. Figure 12 shows the variation of equivalent stress with circumferential position for both designs, with the yield strength at 889 MPa marked. The calculations show clearly that the final design reduces the stress significantly. At the most critical location, the original geometry leads to an equivalent stress above the elastic limit of the material (1140 MPa). The final design features the same narrow slot near the thermocouple bead (to minimize the thermal disturbance at the thermocouple junction), but with a slot expansion at the same depth and a slightly larger hole through the disc. In the final design, the stress

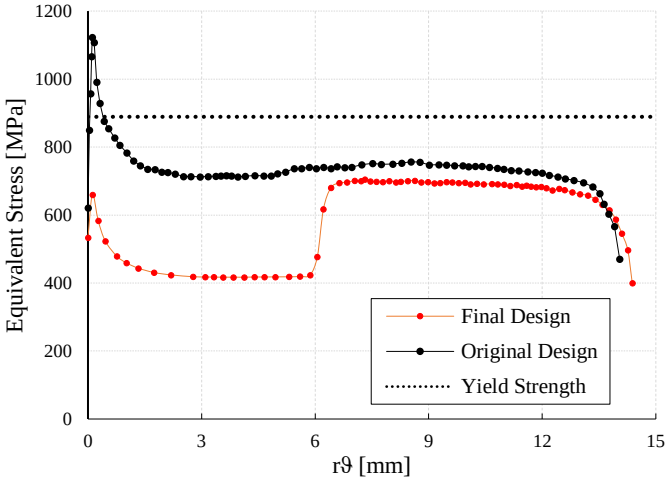

FIGURE 12. Variation of stress with circumferential position for the original and final groove designs.

rise due to the hole is separated from the stress rise due to the circumferential slot, reducing the maximum equivalent stress to 706 MPa, obtaining a safety factor of 1.26. The mechanical load due to rotation alone accounts for ~ 600 MPa.

A fatigue analysis was performed considering 10^4 cycles at conditions of maximum speed and thermal stress. After retrieving the S-N curves, the Soderberg line criterion was used [19], resulting in a fatigue safety factor of 1.37. Samples from the same material batch were tested on a rotating bending machine to confirm the fatigue strength data of the disc material. Linear Elastic Fracture Mechanics (LEFM) [19] was used to estimate the risk associated with crack propagation. A similar approach has been used by Keller [20] on turbine discs. The location with the highest risk was the disc bore (highest *unfeatured* stress). The material was supplied compliant with AMS2631 classA1 (maximum acceptable crack size 1.2 mm) and with standard Dye Penetration Inspection. The discs were bored out by slow wire Electrical Discharge Machining, minimizing the chance of obtaining internal defects. Assuming the maximum surface crack normal to the bore surface (again worst-case scenario), the LEFM analysis yielded a life of ~ 6500 cycles. Note that detailed visual inspections revealed no defects.

6 COMMISSIONING AND TESTING

6.1 Commissioning

The principal commissioning tests were to establish the rotor-dynamic behavior of the rig and ensure data could be captured through the telemetry system. The instrumented discs were assembled onto the drive unit with the wiring pinned and connected to the telemetry unit. The disc pack was trim-balanced and vibrations monitored over the full operating range (800 to 8000 rpm). The maximum allowable vibration of the front bearing was set at 20 µm peak-to-peak (pk-pk). Dynamic calculations for the super-critical design predicted a potential resonance frequency in the range 3000 – 4000 rpm. The design allowed an adjustment of the stiffness of four springs at the front bearing location (near the discs) to control or damp the vibration response.

The variation of the bearing vibration characteristics is shown against rotational speed in Figure 13 for both acceleration and deceleration. The data was collected over the period of one hour and the peak-to-peak vibration was less than 7 µm. The data reveals a small degree of hysteresis between acceleration and deceleration. Local resonance peaks were detected in the range 5000 – 5500 rpm, and a more significant peak near 7000 rpm. The rotor-dynamic response was considered satisfactory to allow rig operation at all rotational speeds up to 8000 rpm. The vibration data shown in Figure 13 were acquired without the cob attachments; repetition of the tests with the cob attachments revealed no detectable change in the vibration characteristics.
About 70% of the thermocouples on the rotating discs were functioning after the rig commissioning. Most of the losses, however, were encountered in the many handling stages required by the installation rather than the testing itself.

Initial tests of the rig were used to explore steady-state buoyancy-induced flow and heat transfer. So far 33 steady-state

temperature distributions have been measured over a range of Gr, $\beta\Delta T$, Ro and Re_z, all with symmetrical heating to the shrouds. A selection of the collected data is discussed below; further analysis of the data is reported in Jackson *et al.* [15].

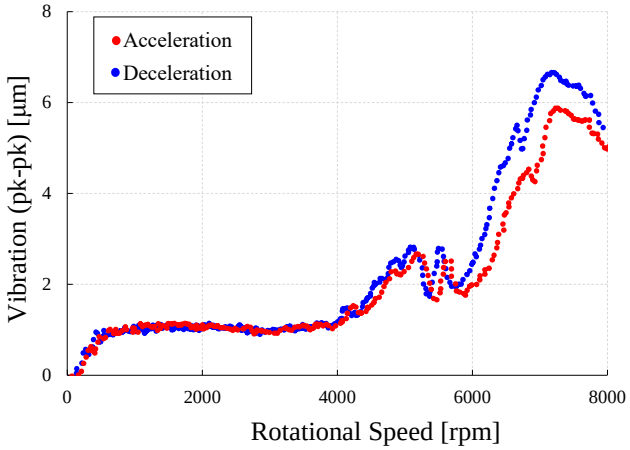

FIGURE 13. Measured peak-to-peak vibrations in rig acceleration and deceleration (post trim balancing). Lines refer to moving average of the collected data.

6.2 Typical temperature measurements

Figure 14 shows the variation of temperature with non-dimensional radius for the following non-dimensional conditions: $Re_\phi = 1.6\times10^6$, $\beta\Delta T = 0.24$, Ro = 0.2 and Gr = 5.9×10^{11}. The silhouette of the central cavity indicates measurement points, which are aligned radially with the data presented.

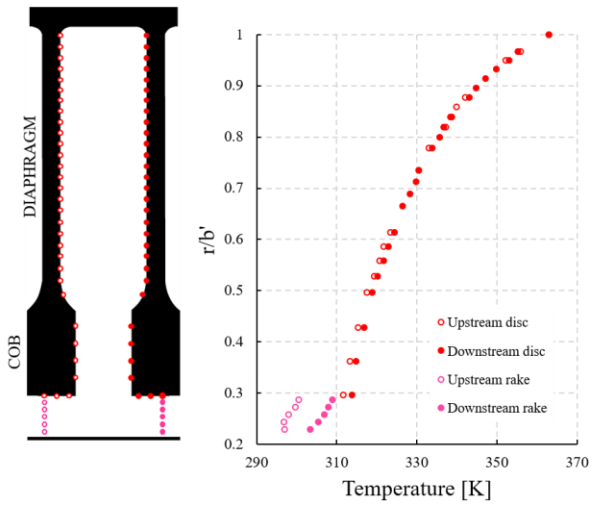

FIGURE 14. Upstream and downstream disc and rake temperatures: $Re_\phi = 1.6\times10^6$; $\beta\Delta T = 0.24$; Ro = 0.2; Gr = 5.9×10^{11}.

The axial throughflow is left-to-right; the closed and open symbols are for data on the upstream and downstream rotating discs respectively. Also shown are the air temperatures of the axial throughflow measured just upstream and downstream of the rotating cavity. The temperature rise of the axial throughflow is caused by heat transfer from the rotating surfaces to the throughflow. As shown in Figure 1, there is a forced convection region between the throughflow and the core. Referring to Figure 14, at the larger radii ($r/b > 0.6$), towards the shroud and for most of the diaphragm, the differences between the temperatures of the upstream and downstream discs temperatures on the upstream and downstream discs are virtually the same, the average is used to create a radial distribution for each condition.

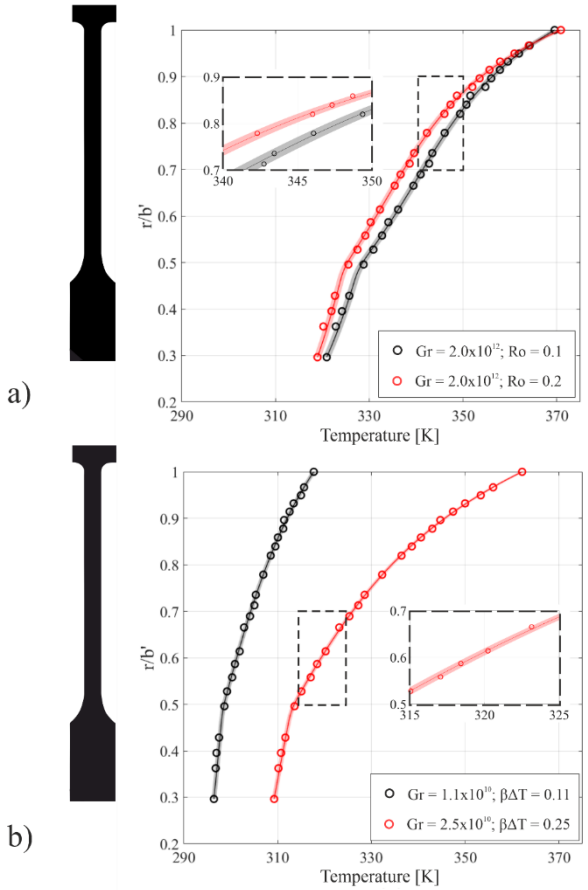

FIGURE 15. Effect of (a) Rossby number, and (b) $\beta\Delta T$ on the radial temperature distribution, at two different magnitudes of Gr. 95% confidence bounds are shown on the Bayesian distribution. The inset figures show a magnified portion of the curve. For (a), $Re_\phi = 3.0\text{x}10^6$, Gr = $2.0 \text{ x } 10^{12}$ and $\beta\Delta T = 0.22$. For (b), $Re_\phi = 3.2\text{x}10^5$, Gr ~ 10^{10} and Ro = 0.5.

Although the estimated uncertainty in individual thermocouple measurements was ± 0.5° C, it is more meaningful - as stated in Section 3 - to consider the uncertainty in the disc tempertures estimated from the Bayesian model used in [15]. The radial distribution of disc temperatures and the standard deviation obtained from the Bayesian model are show in Figure 15. (It is shown in [15] that the uncertainty in the Nusselt numbers is much larger than that in the temperatures.) It should

be noted that, as the temperature difference between the two discs was very small, the average values are used in this figure.

Figure 15a shows the effect of Rossby numbers for a Grashof number of 2.0 x 10^{12}, where the standard deviation in the temperature was approximately 0.4°C. The higher Ro increases the forced convection in the cob region, resulting in lower temperatures, especially at low radius. An increase in Ro does not significantly change the profile of the temperature gradient, as the buoyancy forces are constant. However, as the throughflow acts as a stronger heat sink with more enthalpy transfer, the temperatures on the discs are reduced. Figure 15b shows the effect of $\beta\Delta T$ for a rotational Reynolds number of 3.2 x 10^5 where the standard deviation was approximately 0.25°C. Although an approximate doubling of $\beta\Delta T$ has a large effect on the temperature distribution, this is primarily due to the fact that the temperature of the shroud has been doubled.

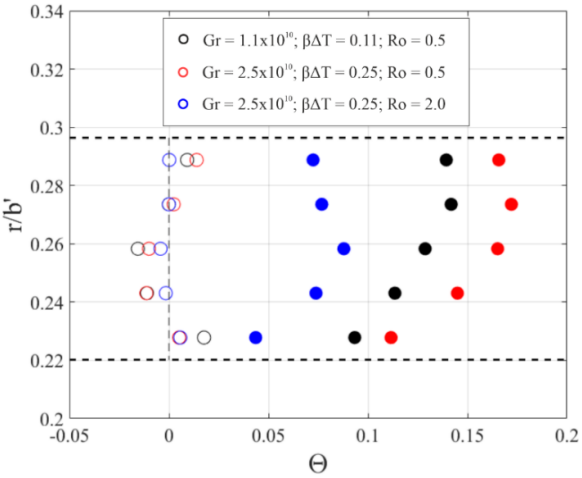

FIGURE 16. Effect of $\beta\Delta T$ and Rossby number on the radial temperature distribution in the axial throughflow upstream and downstream of the test cavity. Refer to Figure 14 for locations of the rakes. Re_ϕ = 3.2x10^5.

Figure 16 shows typical radial distributions of Θ, the non-dimensional temperature of the axial throughflow, which is defined as

$$\Theta = \frac{T_o - T_f}{T_{o,b'} - T_f} \qquad (6)$$

where T_f is the upstream average temperature of the throughflow, T_0 is the local throughflow temperature, and $T_{0,b}$ is the disc temperature at $r = b$. As expected, Θ increases as $\beta\Delta T$ increases and as Ro (which is proportional to the flow rate) decreases. The turning point in the downstream distributions of temperature is attributed to the mixing between the cold throughflow and the heated recirculating flow in the inner region of the cavity. As part of the ongoing research programme, the throughflow temperatures will be used to provide a heat balance between the heat transfer from the rotating surfaces and the enthalpy rise of the throughflow.

7 CONCLUSIONS

The Bath Compressor Cavity Rig has been designed to investigate the buoyancy-induced heat transfer that occurs inside the compressor rotors of aero-engines. The test section includes four rotating discs enclosing three cavities; the central cavity is instrumented with thermocouples and the outer cavities are thermally insulated. There is an axial throughflow of air between a stationary central shaft and the bore of the discs. For a cold throughflow, the outer shroud of the central cavity is heated by two radiant heaters, which allows different shroud temperatures on the upstream and downstream discs. The throughflow can be heated to investigate cases with negative Grashof numbers, which can occur during engine accelerations and decelerations when the throughflow is hotter than the shroud. As stratified flow could occur under these conditions - significantly reducing convection in the cavity so that radiation could be dominant - all internal surfaces of the cavity were painted matt black; this allows the accurate calculation of the radiant heat transfer.

Modularity and flexibility have been addressed in the design of the rig. A rail system allows movement of the disc pack relative to the drive unit and access to the test section. Separate attachments can be fitted to the cobs of both central discs; the attachments reduce the axial gap between the cobs - reducing the gap to zero creates a closed cavity, which can occur in some compressor designs.

Both titanium discs forming the central cavity featured a radial distribution of 28 thermocouples across the cob and diaphragm regions. The thermocouples were located in circumferential slots designed to minimise stress concentrations and thermal disturbance. Thermal and mechanical finite-element stress analysis was used to quantify the stress raisers associated with the machined features and to predict the disc life. Other instrumentation on the rotating discs included heat-flux gauges and high-frequency pressure transducers. Attention has been given to experimental errors, including the computation of thermal-disturbance errors, caused by thermocouples embedded in the rotating discs, and the use of a Bayesian model to reduce the effect of uncertainties in temperature measurements on the calculation of Nu.

In non-dimensional terms, the rig can operate over the range $-1.2\times10^{12} < Gr < 2\times10^{12}$, $0.1 < Ro < 0.8$, and up to $Re_\phi = 3\times10^6$, $Re_z = 4\times10^4$ and $\beta\Delta T = 0.25$. The effect of Ro and $\beta\Delta T$ on the radial distribution of both the disc and throughflow temperatures has been shown for some typical cases. Disc temperatures measured on the rig are used in [15] to determine the effect of Re_ϕ, Ro and $\beta\Delta T$ on the radial distribution of Nu. As part of the ongoing research programme, the throughflow temperatures will be used to provide a heat balance between the heat transfer from the rotating surfaces and the enthalpy rise of the throughflow.

ACKNOWLEDGEMENTS

This work was supported by the UK Engineering and Physical Sciences Research Council, under the grant number EP/P003702/1 in collaboration with the University of Surrey. The authors wish to thank Jas Van Milligan, Martin McNulty, Adam Kitchener and Anshuman Gupta of Torquemeters Ltd.

(Northampton, UK) for their support in the design and construction of the test rig. The authors also thank Prof AB Turner, University of Sussex, for his help and advice with respect to the instrumentation on the rig.

REFERENCES

[1] Owen, J. M. and Long, C.A. 2015 "Review of buoyancy-induced flow in rotating cavities", ASME J Turbomach., 137(11), p. 111001.
[2] Günther, A., Uffrecht, W., Odenbach, S., 2012, "Local measurements of disc heat transfer in heated rotating cavities for several flow regimes", ASME J Turbomach., 134(5), p. 051016.
[3] Günther, A., Uffrecht, W., Odenbach, S., 2014, "The effects of rotation and mass flow on local heat transfer in rotating cavities with axial throughflow", ASME paper GT2014-26228.
[4] Quan, Y., Han, D., Xu, G., Wen, J., Luo, X., 2018, "Convective heat transfer of a rotating multi-stage cavity with axial throughflow", Int. J. Heat and Mass Transfer, 119, p. 117-127.
[5] Diemel, E., Odenbach, S., Uffrecht, W., Rey Villazon, J., Guijarro Valencia, A., Reinecke, M., 2019, "High speed single cavity rig with axial throughflow of cooling air: rig structure and periphery", ASME paper GT2019-91265.
[6] Alexiou, A., 2000, "Flow and heat transfer in gas turbine H.P. compressor internal systems", D.Phil. Thesis, School of Engineering, University of Sussex, UK.
[7] Long, C. A., Miche, N. D. D., and Childs, P. R. N., 2007, "Flow measurements inside a heated multiple rotating cavity with axial throughflow," Int. J. Heat Fluid Flow, 28(6), p. 1391–1404.
[8] Long, C. A., and Childs, P. R. N., 2007, "Shroud heat transfer measurements inside a heated multiple rotating cavity with axial throughflow," Int. J. Heat Fluid Flow, 28(6), p. 1405–1417.
[9] Long, C. A., Alexiou, A., and Smout, P. D., 2003, "Heat transfer in H.P. compressor internal air systems: measurements from the peripheral shroud of a rotating cavity with axial throughflow," 2nd International Conference on Heat Transfer, Fluid Mechanics and Thermodynamics (HEFAT 2003), Victoria Falls, Zambia, June 23–25, Paper No. LC1.
[10] Miché, N. D., 2008, "Flow and heat transfer measurements inside a heated multiple rotating cavity with axial throughflow", D.Phil. Thesis, School of Engineering, University of Sussex, UK.
[11] Atkins, N. R., Kanjirakkad, V., 2014, "Flow in a rotating cavity with axial throughflow at engine representative conditions", ASME paper GT2014-271747.
[12] Tang, H., Shardlow, T., and Owen, J.M., 2015, "Use of fin equation to calculate Nusselt numbers for rotating discs," ASME J. Turbomach., 137(12), p. 121003.
[13] Bohn, D., Deutsch, G., Simon, B., and Burkhardt, C., 2000, "Flow visualisation in a rotating cavity with axial throughflow", ASME Paper No. 2000-GT-0280.
[14] Burkhardt, C., Mayer, A. and Reile, E., 1992, "Transient thermal behaviour of a compressor rotor with axial cooling air flow and co-rotating or contra-rotating shaft", AGARD CP527, p. 21.1-21.9.
[15] Jackson, R. W., Luberti, D., Tang, H., Pountney, O. J., Scobie, J. A., Sangan, C. M., Owen, J. M., Lock, G. D., 2020, "Measurement and analysis of buoyancy-induced heat transfer in aero-engine compressor rotors", ASME paper GT2020-14427.
[16] Tang, H., Puttock-Brown, M. R., and Owen, J. M., 2018, "Buoyancy-Induced Flow and Heat Transfer in Compressor Rotors", *ASME J. Eng. Gas Turb. Power*, **140**(7).
[17] Dorfman, L. A., 1963, "Hydrodynamic resistance and the heat loss of rotating solids", Oliver & Boyd.
[18] Owen, J. M., and Tang, H., 2015, "Theoretical model of buoyancy-induced flow in rotating cavities", ASME J. Turbomach., 137(11), p. 111005.
[19] Budynas, R. G. and Nisbett, J. K., 2010, "Shigley's Mechanical Engineering Design", McGawHill, 9th Edition.
[20] Keller, S., 2015, "A practical approach to implementing linear elastic fracture mechanics in gas turbine rotor disk analyses", ASME Paper No. GT2015-43303.

APPENDIX 1 THERMAL-DISTURBANCE ERROR

The thermal-disturbance error is the difference between the undisturbed surface temperature and the temperature measured by the embedded thermocouple bead. It depends on the heat flux and on the ratio of the thermal conductivity of the thermocouple wires, together with the adhesive surrounding them, to that of the titanium disc. It should be noted that the disturbance error is a bias and not a random uncertainty in the temperature measurement.

In the experimental rig, the narrow part of the slot containing the thermocouple bead was 0.5 mm wide and 0.5 mm deep. The chromel and alumel wires were 0.13 mm diameter, with thermal conductivities taken as 19 and 30 W/mK respectively, and the bead diameter was less than 0.4 mm. The wires and bead were bonded into the slot using an epoxy adhesive (Loctite EA9497) with a thermal conductivity of 1.4W/mK according to the manufacturer. The surface of the epoxy was made flush with that of the titanium disc (k = 7 W/mK).

The disturbance error was modelled with a steady finite-element analysis (FEA) using the ANSYS v18.1 code, and the geometry, based on a 3D segment of the disc containing a thermocouple slot, is shown in Figure A1. The unstructured mesh contained 1.69 million elements; the sizes of the elements were 1.5 mm for the disc, 0.08 mm for the slot material and for the disc surfaces in contact with that material, and 0.03 mm at the curved tip of the slot. The effective thermal conductivity of the slot material was assumed to be the volume-weighted-average of the conductivities of the wires, the bead and the adhesive. Three cases were considered for the slot conductivity: pure adhesive (k = 1.4 W/mK); wires and epoxy (k = 3.82 W/mK); bead and epoxy (k = 12.9 W/mK).

The temperatures of the inner and outer surfaces of the segment were 20° C and 100° C respectively, and the underside

and edges of the segment were assumed to be adiabatic. The heat transfer coefficients onto the top surface were calculated using the buoyancy model described in Section 2, based on the maximum rotational speed of 8000 rpm. As the radial location of the slot was the same as that of the outermost thermocouple on the disc, the thermal disturbance error was assumed to be the maximum that would be experienced during the experiments.

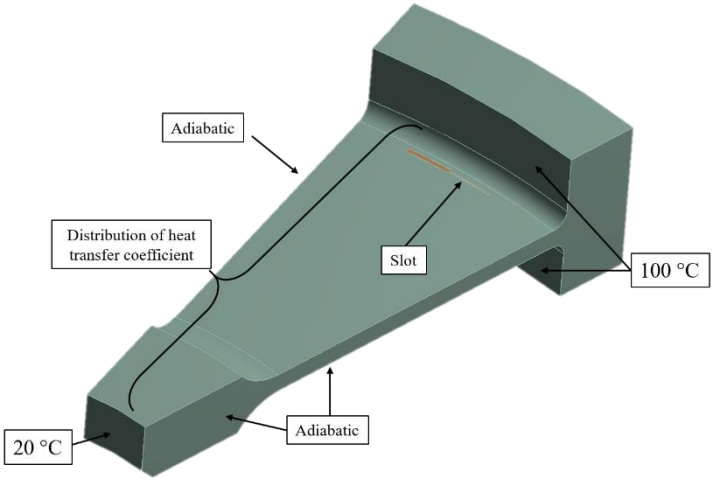

FIGURE A1. Boundary conditions of the FEA model.

The computed angular distribution of surface temperature at the radial centre and circumferential edge of the slot is shown in Figure A2 for the three effective slot conductivities referred to above. For the pure epoxy case (k = 1.4 W/mK), the *magnitude* of the disturbance of the temperature of the slot surface is a maximum (0.24 ºC); as the heat transfer is from the disc to the air, the surface temperature of the slot is *lower* than that of the undisturbed temperature. For the wires and epoxy (k = 3.82 W/mK), the maximum magnitude is 0.049 ºC. For the bead and epoxy (k = 12.9 W/mK), the maximum magnitude is 0.025 ºC; for this case, where the slot has a higher conductivity than the substrate, the surface temperature of the slot is *higher* than that of the undisturbed temperature. (It can be seen that the three asymptotic temperatures in the substrate away from the slot differ by a very small amount, < 0.05 ºC. This difference is caused by the fact that the temperature of the substrate has been altered by the presence of the slot material.)

It is considered that 0.24 ºC is a conservative maximum and the actual error will be less than this. At the other radial locations and for lower heat fluxes, the errors will be even smaller and therefore insignificant.

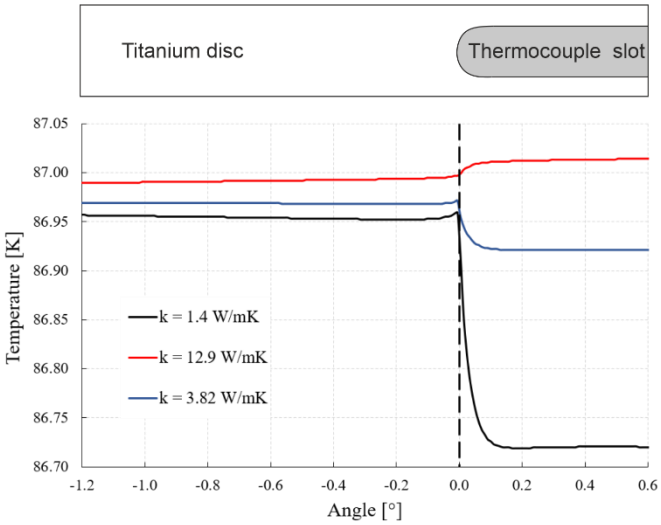

FIGURE A2. Effect of slot conductivity on computed angular distribution of surface temperature distribution

APPENDIX 2 INSTRUMENTATION

	TC (K-type, in-house welding)	**TC** (K-type, thin foil)	Heat Flux Sensors	Static Pressure	Unsteady Pressure
Shaft				**5** *(many axial locations)*	
Annulus	**10** *(5 per rake, one rake per disc)*				
Bore D2		**3**	**1**		
Bore D3		**3**			
Diaphragm D2	**28**				
Diaphragm D3	**28**				**2**
Shroud D2		**3**	**1**		
Shroud D3		**3**	**1**		
Outer Shroud D2	**1**				
Outer Shroud D3	**1**				
TOTAL	**68**	**12**	**3**	**5**	**2**